Embryonic Protein Nodal Promotes Breast Cancer Vascularization

Daniela F. Quail[1], Logan A. Walsh[3], Guihua Zhang[1], Scott D. Findlay[1], Juan Moreno[4], Laura Fung[5], Amber Ablack[5], John D. Lewis[6], Susan J. Done[4], David A. Hess[2], and Lynne-Marie Postovit[1]

Abstract

Tumor vascularization is requisite for breast cancer progression, and high microvascular density in tumors is a poor prognostic indicator. Patients bearing breast cancers expressing human embryonic stem cell (hESC)-associated genes similarly exhibit high mortality rates, and the expression of embryonic proteins is associated with tumor progression. Here, we show that Nodal, a hESC-associated protein, promotes breast cancer vascularization. We show that high levels of Nodal are positively correlated with high vascular densities in human breast lesions ($P = 0.0078$). *In vitro*, we show that Nodal facilitates breast cancer–induced endothelial cell migration and tube formation, largely by upregulating the expression and secretion of proangiogenic factors by breast cancer cells. Using a directed *in vivo* angiogenesis assay and a chick chorioallantoic membrane assay, we show that Nodal promotes vascular recruitment *in vivo*. In a clinically relevant *in vivo* model, whereby Nodal expression was inhibited following tumor formation, we found a significant reduction in tumor vascularization concomitant with elevated hypoxia and tumor necrosis. These findings establish Nodal as a potential target for the treatment of breast cancer angiogenesis and progression. *Cancer Res; 72(15); 3851–63. ©2012 AACR.*

Introduction

Metastatic breast cancer cells exhibit stem cell–like properties (1, 2) and the expression of hESC-associated genes is associated with poor prognosis in breast cancer patients (3, 4). Nodal, a morphogen from the TGF-β superfamily, is a hESC-associated protein that becomes reexpressed during cancer progression (1, 5–7). Nodal signals via a SMAD2/3-dependent pathway following activation of a receptor complex, including ALK4/7, ActRIIB, and the coreceptor Cripto-1 (8). Recent studies show that Nodal promotes a dedifferentiated phenotype in melanoma, glioma, prostate cancer, and pancreatic cancer and that it increases cancer cell invasion and tumorigenicity in these cancer types (5, 7, 9, 10). Nodal expression is also correlated with breast cancer progression, such that Nodal is absent in normal breast tissues, yet is aberrantly expressed in invasive breast cancer lesions (6).

Authors' Affiliations: [1]Department of Anatomy & Cell Biology, University of Western Ontario; [2]Department of Physiology & Pharmacology and Robarts Research Institute, London, Ontario, Canada; [3]Human Oncology and Pathogenesis Program, Memorial Sloan Kettering Cancer Center, New York, New York; [4]Campbell Family Institute for Breast Cancer Research, University Health Network, Toronto, Ontario; [5]Innovascreen, Inc., Halifax, Nova Scotia; and [6]Department of Oncology, University of Alberta, Edmonton, Alberta, Canada

Note: Supplementary data for this article are available at Cancer Research Online (http://cancerres.aacrjournals.org/).

Corresponding Author: Lynne-Marie Postovit, Department of Anatomy & Cell Biology, Schulich School of Medicine & Dentistry, University of Western Ontario, Medical Sciences Building, Rm. 438, London, Ontario, Canada, N6A 5C1. Phone: 519-661-2111 (ext. 80524); Fax: 519-661-3936; E-mail: Lynne.Postovit@schulich.uwo.ca

doi: 10.1158/0008-5472.CAN-11-3951

The acquisition of stem cell markers has been linked to the enhancement of hallmarks of cancer, such as self-sufficiency in growth signals and cellular invasion. Angiogenesis has also been correlated with the acquisition of stem cell markers. For example, $CD105^+$ human renal carcinoma cells, expressing Nestin, Nanog, and Oct3/4, promote angiogenesis by shedding microvesicles that contain mRNAs for proangiogenic growth factors (11). In addition, a mesenchymal-like subclass of high-grade gliomas has been shown to exhibit elevated expression of proangiogenic factors, including VEGF and PECAM (CD31), and a recent study revealed that glioma stem cell–like populations promote vascularization via a combinatorial mechanism involving the secretion of VEGF and stromal derived factor-1 (12, 13). Lastly, one study has reported that Nodal regulates VEGF expression and vessel density in gliomas (14). However, this latter study did not directly assess the role of Nodal in the regulation of angiogenesis or vasculogenesis.

Here, we show that Nodal protein is correlated with high microvascular density in human breast cancer tissues, and that it causes vascular recruitment *in vivo*. *In vitro*, we found that Nodal increases the ability of breast cancer cells to promote tube formation by endothelial cells, and that it regulates the expression of VEGF and PDGF in these breast cancer cells. Finally, using inducible short hairpin RNAs (shRNA), we determined that Nodal can be targeted in established tumors to decrease vascular density and induce necrosis. In adults, Nodal is largely tumor specific; hence, it may be a useful target for the treatment of breast cancer.

Materials and Methods

Please see Supplementary Data for full methods.

Ethics statement

Tissue was obtained from the Ontario Tumor Bank. Experiments involving animals were approved by the Animal Use Subcommittee at the University of Western Ontario (Protocol no. 2008-101).

Evaluation of Nodal and vascular density

Immunohistochemistry (IHC) for Nodal or CD31 was conducted using antibodies as described (Supplementary Table S1). To verify the specificity of Nodal staining, monoclonal and polyclonal antibodies were compared (Supplementary Fig. S1). In confirmation with previous studies, these antibodies revealed comparable staining patterns (15). We proceeded with the monoclonal antibody, as previously described (5, 6, 16). Cytoplasmic staining for Nodal was seen in all cases. Stained sections were blindly and independently scored by 2 pathologists (S.J. Done and J. Moreno) to derive an Allred score (17). Values were dichotomized using a total Allred score of 7 and 8 as high expression and 6 or less as low expression. Microvascular density (MVD) was blindly and independently scored based on CD31 immunohistochemical staining, following the recommendations from the International Consensus on Evaluation of Angiogenesis in Solid Human Tumors (18). Data were dichotomized using the average number of vessels among all samples as the cutoff between high and low MVD values. All scoring values obtained by S.J. Done and J. Moreno had a Pearson correlation coefficient (rp) of 0.73 or higher. A total of 83 cases of 90 had both Nodal and CD31 MVD scores, which were used for statistical analyses. For clinical characteristics of these 83 patients, see Supplementary Table S2. Assessment of correlations was carried out using Pearson correlation and a 2-sided *t* test.

Cell culture and transfection

Human umbilical vein endothelial cells [HUVEC; American Type Culture Collection (ATCC)], and primary human adult microvascular endothelial cells (HMVECs; Invitrogen) were maintained as per instructions. All breast cancer cell lines were obtained from and validated by ATCC and were maintained as per instructions. Multiple constructs were used to knockdown or induce Nodal signaling in each of the cell lines used (Supplementary Methods).

RNA extraction and reverse transcriptase PCR

Total RNA was isolated and reverse transcriptase PCR (RT-PCR) was carried out using human primer/probe sets (Supplementary Table S3).

Western blotting

Protein lysates were prepared and Western blotting was conducted as previously described (6) using appropriate antibodies (Supplementary Table S1). In accordance with previous studies (5, 6, 19, 20), up to 3 Nodal species were detected: pro-Nodal bands at approximately 39 kDa, multiple processed (glycosylated etc.) bands at approximately 50 kDa, and a cleaved Nodal band at approximately 15 kDa. These bands are proportionally expressed (20).

In vitro functional assays

Tube formation, migration, viability, and proliferation were assayed. In some cases, rhNodal (100 ng/mL; R&D), VEGF (20 ng/mL; Invitrogen), and/or platelet-derived growth factor (PDGF; 20 ng/mL; Invitrogen) were added to the conditioned medium after it was collected. An amount of 20 ng/mL of VEGF and PDGF was used in accordance with previous reports (21, 22).

Measurement of angiogenic proteins

VEGF and PDGF were measured using Aushon SearchLight Chemiluminescent Angiogenesis Arrays (#84694; Aushon Biosystems) or by Western blot analysis.

Directed *in vivo* angiogenesis assay

In vivo angiogenesis assays (Trevigen) were carried out as per instructions.

Chorioallantoic membrane tumor angiogenesis assay

One collagen-enmeshed grid containing 2×10^6 cells was placed on each chorioallantoic membrane (CAM), and newly formed blood vessels were scored and quantified as previously described (23).

In vivo tumor assay

MDA-MB-231 cells were transfected with a doxycyclin-inducible control or Nodal-targeted shRNA. A total of 500,000 cells were injected into the flank of 6- to 8-week-old female Nude mice (Crl:NU-*Foxn1*^{nu}; Charles River). Doxycyclin was administered 2 weeks following onset of palpable tumors via diet (0.625 g doxycyline hyclate/kg; Harlan Laboratories). Immunofluorescence for CD31 and Nodal was conducted, and RNA was extracted to measure the expression of *VEGF* and *PDGF*. To assess necrosis, 3 tumor sections spaced evenly through tissue block were stained with hematoxylin and eosin (H&E). Necrosis was calculated as a percentage of the total tumor area. To assess hypoxia, animals were injected with hypoxyprobe-1 (60 mg/kg) and IHC for hypoxyprobe adducts was carried out on tissue sections.

Statistical analyses

Multiple comparisons for parametric data were carried out using one-way ANOVA and a Tukey–Kramer Comparisons Post-Hoc test. ANOVA on ranks and a Mann–Whitney rank sum test were used for nonparametric data. Student *t* test was used to compare 2 variables. All statistical tests were 2-sided and comparisons were considered statistically significant at $P < 0.05$.

Results

Nodal correlates with microvascular density in human breast cancers

Angiogenesis is a rate-limiting step in the metastatic cascade, and high MVD is correlated with a poor clinical outcome (24, 25). Given recent evidence linking tumor angiogenesis to stem cell markers, we sought to determine whether Nodal expression correlates with MVD in human breast cancers. Immunohistochemical analysis of Nodal and CD31 (to

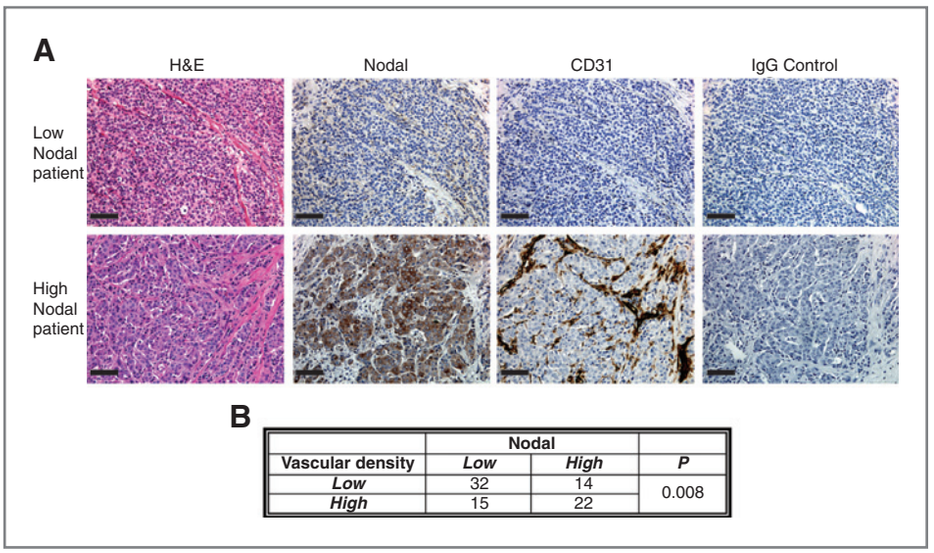

B

	Nodal		
Vascular density	*Low*	*High*	*P*
Low	32	14	0.008
High	15	22	

Figure 1. High Nodal expression is associated with a high vascular density in breast cancer lesions. A, immunohistochemical staining (brown) of Nodal and CD31 in serial sections of human breast cancers. Examples of patients with low and high levels of Nodal expression are displayed. Sections stained with H&E or an isotype control are also included. Bar equals 50 μm. B, entire sections of each breast cancer case were analyzed to derive an Allred score for Nodal expression. A total Allred score of 7 and 8 represented high Nodal expression and a score of 6 and below represented low Nodal expression. In serial sections, vascular density was scored based on CD31 staining. Vessel density was dichotomized using the average number of vessels among all the samples as the cutoff between high and low vascular density values. High Nodal expression is associated with a high vascular density in human breast cancers ($n = 83$, rp = 0.3, $P = 0.0076$).

demarcate endothelial cells) in breast cancer patients was examined using serial sections (25). Breast cancer tissue from 90 patients was procured from the primary tumor site; 89 via surgical resection and 1 via excisional biopsy. The average age of the patients was 61 years (ranging from 27–90). The majority of the cases were invasive disease, diagnosed as being grade 3 (47%) or grade 2 (37.4%). Of the 90 samples, 83 could be scored for both Nodal and MVD and were used for statistical analyses. Clinical characteristics of these patients are listed in Supplementary Table S2. IHC for both Nodal and CD31 was heterogeneous, varying among individuals and within sections in extent, intensity, and localization. Nodal was generally confined to epithelial-like tumor cells (Fig. 1A; Supplementary Figs. S1 and S2). Nodal staining was not correlated to breast cancer grade ($P = 0.140$) or to estrogen receptor (ER) ($P = 0.682$), progesterone receptor (PR; $P = 0.801$) or HER-2 ($P = 0.589$) status. However, high levels of Nodal were associated with a high VD ($n = 83$; rp = 0.3, $P = 0.0076$), suggesting a clinical association between the acquisition of Nodal expression and vascular recruitment (Fig. 1A and B; Supplementary Fig. S2).

Nodal promotes a proangiogenic niche

To explore whether Nodal regulates breast cancer angiogenesis, we first tested the effects of Nodal on endothelial cell tube formation and migration using HUVECs or HMVECs treated with conditioned media from stably transfected breast cancer cells. For our loss-of-function experiments, we used MDA-MB-231 cells, which express high levels of Nodal, and for our gain-of-function approach, we used T47D cells, which express relatively low levels of Nodal (Fig. 2A; ref. 6). We found that conditioned media from MDA-MB-231 cells transfected with a Nodal-targeted shRNA (231+shNodal) significantly reduced endothelial branching (HUVEC, $n = 3$, $P < 0.001$; HMVEC, $n = 3$, $P < 0.001$) and migration (HUVEC, $n = 4$, $P < 0.001$; HMVEC, $n = 3$, $P < 0.001$) compared with conditioned media from MDA-MB-231 cells expressing a control shRNA (231+shControl; Fig. 2B–E, H–J). This effect was not due to altered cell viability or proliferation (Fig. 2F, G, K). In complementary Nodal gain-of-function experiments, we treated HUVECs with conditioned media from T47D cells transfected with an empty vector (T47D+EV) or a Nodal expression construct (T47D+Nodal; Fig. 2L). We found that tube formation ($n = 3$, $P < 0.01$) and migration ($n = 4$, $P < 0.05$) were significantly increased in response to conditioned media from T47D+Nodal cells, compared with T47D+EV cells (Fig. 2M–O). This effect was not due to a change in viability (Fig. 2P).

To determine whether Nodal was acting directly on the endothelial cells or indirectly by regulating the expression of angiogenic factors in the cancer cells, we added recombinant human Nodal (rhNodal) to the collected conditioned media during the course of the tube formation assays. Although migration of HUVECs was rescued by rhNodal treatment, migration of HMVECs and tube formation for both endothelial cell types were not affected (Fig. 2C–F, H–K). This suggests that Nodal acts on some endothelial cells directly, but that Nodal also promotes angiogenesis indirectly, perhaps by upregulating the secretion of proangiogenic proteins by the cancer cells.

In support of this concept, although Nodal inhibition with shRNA did not significantly alter cellular proliferation of MDA-MB-231 when conditioned medium was collected, it did cause a significant reduction in PDGF ($n = 3$, $P = 0.018$) and VEGF ($n = 3$, $P = 0.007$) protein (Fig. 3A–D). Furthermore, addition

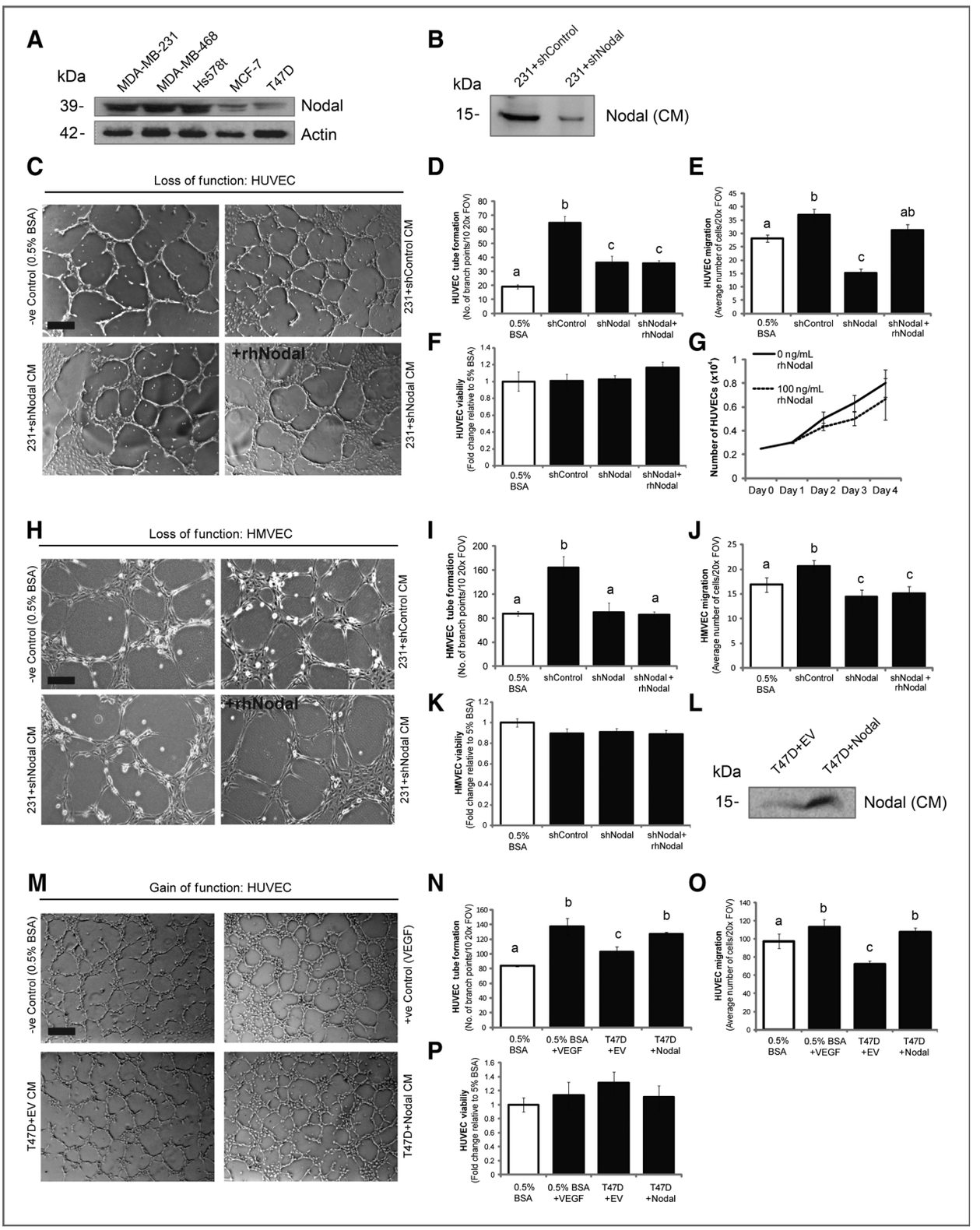

Figure 2. Nodal promotes a proangiogenic niche. A, Western blot comparing Nodal expression across MDA-MB-231, MDA-MB-468, Hs578t MCF-7, and T47D breast cancer cell lines. Pro-Nodal (~39 kDa) is presented and actin is used as a loading control. B, Western blot of Nodal protein in conditioned medium of 231+shNodal cells or 231+shControl cells. The approximately 15 kDa cleaved and secreted Nodal band is presented. C, representative images of

of rhNodal (100 ng/mL) to 231+shNodal cells rescued VEGF expression in these cells (Fig. 3E). To validate these observations, we measured VEGF and PDGF protein in response to Nodal knockdown in MDA-MB-468 cells using a protein array. We found that Nodal inhibition caused decreased expression of PDGF and VEGF in conditioned media ($n = 3$, $P < 0.03$) and cell lysate ($n = 3$, $P < 0.001$; Fig. 3F–J). In complementary gain-of-function experiments, treatment of T47D cells with rhNodal did not affect cellular proliferation (Fig 3K and L) but did cause a significant increase in *VEGF* and *PDGF* mRNA expression ($n = 3$, $P < 0.05$; Fig. 3M). Furthermore, treatment of T47D or MCF-7 cells with increasing concentrations of rhNodal (0, 50, or 100 ng/mL) resulted in an increase in VEGF and PDGF protein expression (Fig. 3N). Similarly, using a protein array, we found that transfection of T47D cells with a Nodal expression construct caused a significant increase in PDGF protein expression in conditioned media ($n = 3$, $P = 0.045$) and cell lysate ($n = 4$, $P = 0.029$; Fig. 3O and P) and a significant increase in VEGF protein expression in cell lysate ($n = 3$, $P = 0.029$; Fig. 3Q–S). Lastly, we found that activation of Nodal type I receptor is required for VEGF and PDGF regulation, as treatment of T47D cells with SB431542 inhibited rhNodal-induced upregulation of these proteins (Fig. 3T).

We next investigated whether we could rescue the effects of shNodal-conditioned media on endothelial cells with recombinant VEGF and/or PDGF. We added these proteins to the conditioned media after it was collected from the cancer cells (i.e., during the incubation on endothelial cells). Unlike the addition of rhNodal, which did not rescue angiogenic phenotypes, we found that addition of VEGF and/or PDGF to 231+shNodal conditioned media during the tube formation and migration assays did restore both phenotypes in HUVEC and HMVEC cultures (Fig. 4A–C, E–G). This was not because of a significant change in viability (Fig. 4D and H).

Nodal promotes vascular recruitment *in vivo*

To test the significance of our *in vitro* results, we carried out Directed In Vivo Angiogenesis Assays (DIVAA). Briefly, cancer cells were seeded into matrix-containing angioreactors, which were implanted subcutaneously into mice. Endothelial cells that invaded the angioreactors were quantified using a fluorescein isothiocyanate–lectin–based assay (26). We determined that 468+shControl cells ($n = 7$, $P = 0.007$) and 231+shControl cells ($n = 10$, $P = 0.003$) efficiently recruit vasculature within 10 days, and that this ability is mitigated when Nodal is knocked down (Fig. 5A–D). Moreover, this *in vivo* effect of Nodal knockdown on angiogenesis was rescued in 468+shNodal cells by the addition of VEGF (Fig. 5C and D). In contrast to our *in vitro* studies, we were able to partially recover the effects of Nodal knockdown with the addition of rhNodal (Fig. 5C and D). This may have been because the cancer cells in the implants responded to the rhNodal by reexpressing VEGF and PDGF. Alternatively, Nodal may affect other proangiogenic cell types *in vivo*, such as hematopoietic stem cells, not accounted for in our endothelial cell assays. In accordance with our *in vitro* studies, T47D+Nodal–transfected cells induced significantly higher vessel recruitment compared with controls ($n = 10$, $P < 0.001$; Fig. 5E and F).

As proof-of-principle, we used a chick CAM assay to assess the role of Nodal during vascularization *in vivo* over a 3-day period (23). We found that 231+shControl cells were able to induce almost 2-fold greater angiogenesis than 231+shNodal cells ($n \geq 37$, $P < 0.001$; Fig. 5G). Furthermore, inclusion of recombinant VEGF (20 ng/mL) with 231+shNodal cells on the CAM resulted in a rescue of the angiogenic phenotype (Fig. 5G). When tumor formation was assayed over 5 days, we found that 231+shNodal cells were unable to form tumors compared with controls (Fig. 5H). Furthermore, despite promoting vascularization, VEGF did not rescue 231+shNodal tumor formation (Fig. 5H), suggesting that Nodal may regulate multiple aspects of tumorigenesis in this model.

Inducible Nodal inhibition following tumor formation reduces vascularization

We next evaluated the effects of targeting Nodal in established tumors. MDA-MB-231 cells transfected with a doxycycline-inducible Nodal shRNA (231+ishN) or Control shRNA (231+ishC) were injected into the flanks of mice. Control (–Dox) groups were given regular chow for the entire experiment, whereas +Dox groups were given chow-containing doxycycline during weeks 2 to 4 of the experiment (after tumor initiation; Fig. 6A and B). By administering doxycycline to animals with established tumors, we avoided significant changes in tumor size between treatments, minimizing confounding effects of tumor growth on our analysis of angiogenesis. Of note, we found no significant difference in tumor size

HUVEC tube formation. Cells were treated with 0.5% BSA, 231+shControl-conditioned media, 231+shNodal-conditioned media, or 231+shNodal-conditioned media + rhNodal. Bar, 100 μm. D, quantified HUVEC tube formation corresponding to C. Bars represent mean number of branch points ± SEM ($n = 3$, $P < 0.001$). E, HUVECs cellular migration in response to treatments from C and D. Bars represent mean number of migrated cells per FOV ± SEM ($n = 4$, $P < 0.001$). F, viability of HUVECs in response to treatment conditions from C–E. Bars represent fold change in fluorescence ± SEM relative to 0.5% BSA control ($n \geq 4$, $P = 0.2$). G, HUVEC proliferation in response to treatment with 100 ng/mL rhNodal. No significant difference was observed for any of the time points ($n = 3$, $P > 0.05$). H, representative images of primary HMVEC tube formation. Cells were treated with 0.5% BSA, 231+shControl-conditioned media, 231+shNodal-conditioned media, or 231+shNodal-conditioned media + rhNodal. Bar, 50 μm. I, quantified HMVEC tube formation corresponding to H. Bars represent mean number of branch points ± SEM ($n = 3$, $P < 0.001$). J, HMVEC cellular migration in response to treatments from H and I. Bars represent mean number of migrated cells per FOV ± SEM ($n = 4$, $P < 0.001$). K, viability of HMVECs in response to the treatment conditions from H–J. Bars represent fold change in fluorescence ± SEM relative to 0.5% BSA control ($n = 6$, $P > 0.05$). L, Western blot validation of elevated Nodal protein in conditioned media from T47D+Nodal versus T47D+EV cells. The approximately 15-kDa mature Nodal band is depicted. M, representative images of HUVEC tube formation in cells treated with 0.5% BSA, 20 ng/mL VEGF-A, T47D+EV-conditioned media, or T47D+Nodal-conditioned media. Bar, 100 μm. N, quantified tube formation corresponding to images in M. Bars represent mean number of branch points ± SEM ($n = 3$, $P < 0.01$). O, HUVEC cellular migration in response to treatments from M and N. Bars represent mean number of migrated cells per FOV ± SEM ($n = 4$, $P < 0.05$). P, viability of HUVECs in response to the conditions from M–O. Bars represent fold change in fluorescence ± SEM relative to 0.5% BSA control ($n = 3$, $P = 0.48$). For all graphs, superscripted letters indicate a statistical difference as specified. BSA, bovine serum albumin; CM, conditioned media; FOV, field of view.

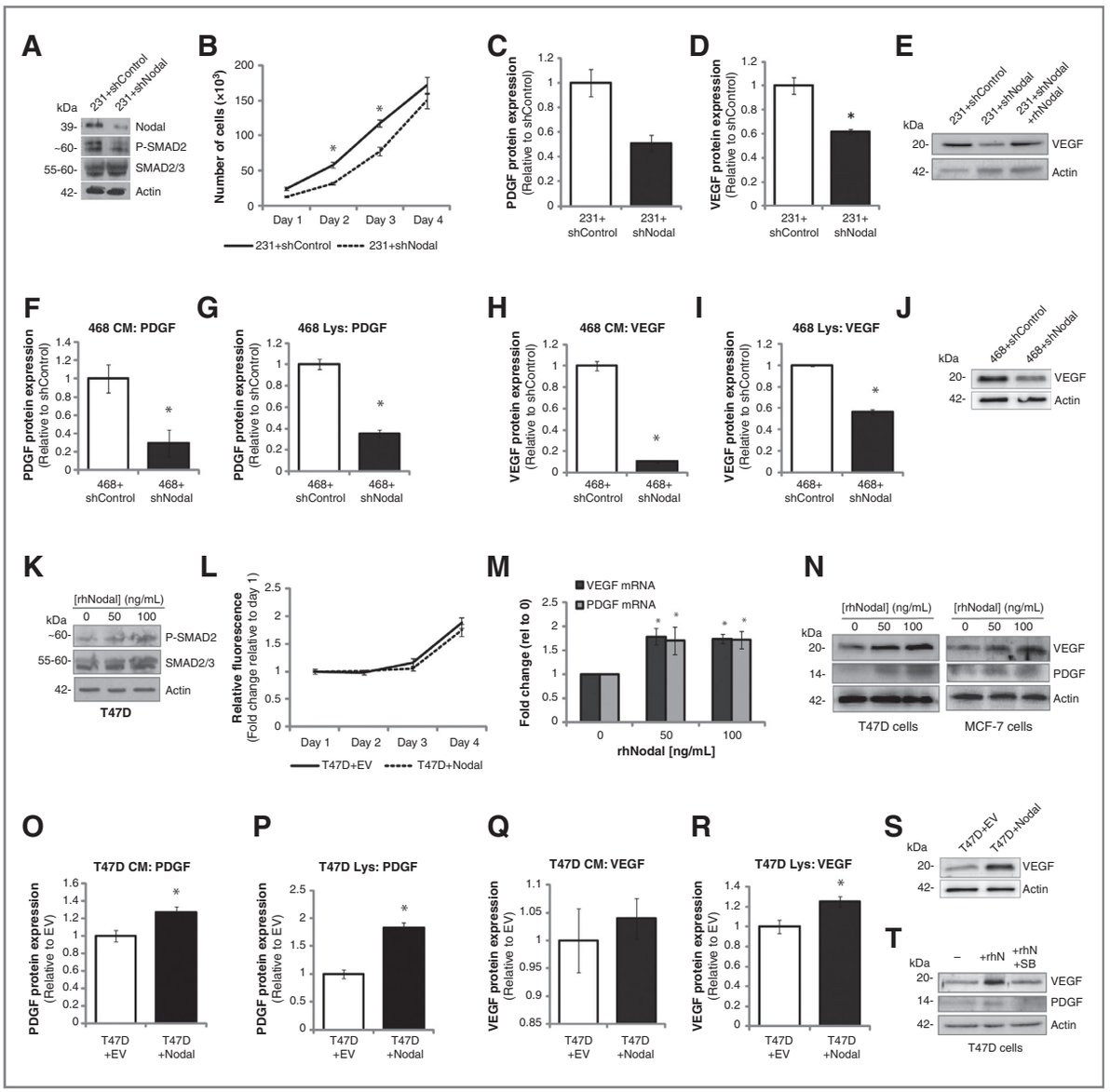

Figure 3. Nodal promotes expression and secretion of proangiogenic factors. A, Western blot validating Nodal knockdown in 231+shNodal versus 231+shControl cells, concomitant with a reduction in phosphorylated-SMAD2. Pro-Nodal (~39 kDa) is depicted and SMAD2/3 and actin are used as loading controls. B, proliferation of 231+shNodal cells and 231+shControl cells. Cell numbers were reduced in 231+shNodal cells at days 2 and 3, but not at day 1 when conditioned medium was taken. C and D, PDGF protein expression (PDGF $n = 3$, $P = 0.018$; C), and VEGF protein expression (VEGF $n = 3$, $P = 0.007$; D) were reduced in 231+shNodal cells compared with 231+shControl cells as measured with a protein array. Bars represent mean protein expression ± SEM. E, Western blot showing a rescue of VEGF protein expression in 231+shNodal cells treated with 100 ng/mL rhNodal. Actin is used as a loading control. F and G, quantification of PDGF protein in conditioned media ($n = 3$, $P = 0.029$; F) or cell lysate ($n = 3$, $P < 0.001$; G) from 468+shControl versus 468+shNodal cells. H and I, quantification of VEGF protein in conditioned media ($n = 3$, $P < 0.001$; H) or cell lysate ($n = 3$, $P < 0.001$; I) from 468+shControl versus 468+shNodal cells. J, Western blot showing reduced VEGF expression in 468+shNodal cells compared with 468+shControl cells. K, Western blot validating dose-dependent induction of Nodal signaling via phospho-SMAD2 in T47D cells in response to vehicle or rhNodal (50 or 100 ng/mL) after 24 hours. Actin was used as a loading control. L, proliferation of T47D+EV versus T47D+Nodal cells showing no significant difference in cell number over a 4-day time course. M, real-time RT-PCR analysis of *VEGF* and *PDGF* expression in T47D cells treated for 24 hours with either vehicle or rhNodal (50 ng/mL, 100 ng/mL). Expression levels are normalized to HPRT1. Bars represent mean gene expression ± SEM relative to 0 ng/mL rhNodal control ($n = 3$, $P < 0.05$). N, Western blot analysis showing a dose-dependent increase in VEGF and PDGF in T47D cells or MCF-7 cells treated with increasing concentrations of rhNodal (0, 50, or 100 ng/mL). Actin is used as a loading control. O and P, quantification of PDGF protein in conditioned media ($n = 3$, $P = 0.045$; O) or cell lysate ($n = 3$, $P = 0.029$; P) from T47D+EV versus T47D+Nodal cells. Q and R, protein quantification of VEGF protein in conditioned media ($n = 3$, $P > 0.05$; Q) or cell lysate ($n = 3$, $P = 0.029$; R) from T47D+EV versus T47D+Nodal cells. S, Western blot showing elevated VEGF expression in T47D+Nodal cells compared with T47D+EV cells. Actin is used as a loading control. T, Western blot showing that VEGF and PDGF are upregulated in response to rhNodal treatment (100 ng/mL) in T47D cells, but that this is mitigated with the addition of SB431542 (10 μmol/L). Actin is used as a loading control. For all graphs, asterisks (*) indicate a significant difference compared with controls as specified. CM, conditioned media.

over time between treatments ($n \geq 4$, $P = 0.4$; Fig. 6C). Following tumor excision, immunofluorescence localization revealed that the distribution of Nodal mirrored the distribution of CD31 across treatments, and that CD31 expression in 231+ishN +Dox tumors was limited to the tumor periphery. Indeed, we found an approximately 50% reduction in CD31 staining in 231+ishN +Dox tumors compared with all other treatments ($n \geq 4$, $P = 0.04$; Fig. 6D and E). In cases in which Nodal expression rebounded following doxycycline treatment in 231+ishN mice (a common limitation of shRNA technology), CD31 expression was similarly restored (Fig. 6F). In accordance with these findings, we found that 231+ishN +Dox exhibited a significant reduction in *VEGF* expression compared with all other treatment groups ($n \geq 3$, $P = 0.003$; Fig. 6G). Significant differences in *PDGF* expression were not, however, detected.

As a corollary to our CD31 and VEGF measurements, we found that tumor necrosis was significantly higher and frequently extended closer to the tumor periphery in 231+ishN +Dox tumors compared with controls ($n \geq 4$, $P < 0.001$; Fig. 7A and B). Furthermore, by injecting mice with Hypoxyprobe-1 before sacrifice and then immunostaining for this compound to delineate low oxygen levels, we determined that hypoxic regions surrounded areas of necrosis, and that 231+ishN +Dox tumors were more hypoxic than control tumors (Fig. 7C).

Discussion

This study shows that the Nodal expression correlates with MVD in human breast cancer tissue, and that this embryonic protein enhances the angiogenic potential of breast cancer cells. Importantly, Nodal can be targeted within growing tumors to inhibit vascularization and promote necrosis. Because vascular density is correlated with metastasis and poor prognosis, our study strongly implicates Nodal as a prognostic indicator and therapeutic target for breast cancer.

In accordance with previous studies in glioma, Nodal promoted VEGF and PDGF expression in all of the human breast cancer cell lines tested (14). However, we found that there were differences in protein expression between lysate and conditioned media within a particular cell type, suggesting that Nodal may be involved in regulation of protein trafficking, protein stability, or secretion. Furthermore, although Nodal was consistent in promoting VEGF and PDGF, a full analysis of a proangiogenic signature was not conducted, leaving the possibility that Nodal may activate other cytokines to mediate vascularization.

When comparing rhNodal rescue treatments from *in vitro* versus *in vivo* experiments, we found that rhNodal differentially rescued the angiogenic phenotype. For instance, addition of rhNodal to shNodal-conditioned media after it was collected from the cancer cells did not rescue tube formation *in vitro*. However, addition of rhNodal to shNodal-containing DIVAA angioreactors did induce a partial rescue of vascularization. This suggests that rhNodal is able to induce signaling and downstream targets when in contact with cancer cells or with other cell types in the animal but is not able to propagate signaling when in contact with only endothelial cells. We speculate that this is due to differential expression of Nodal receptor components, for example, Cripto, across cell types. Although some studies indicate that Nodal may signal in a Cripto-independent manner (27), others suggest that Cripto is required for Nodal-induced phenomena. Moreover, Cripto has been linked to breast and colon tumorigenesis, and one study reported that Cripto promotes HUVEC migration *in vitro* and angiogenesis *in vivo* (28, 29). Future studies exploring patterns of Cripto expression on endothelial cells or endothelial progenitors, and the role of Cripto in Nodal-induced angiogenesis would be valuable for developing targeted therapies.

Although we showed that Nodal induces angiogenesis by regulating proangiogenic factors and promoting endothelial cell recruitment, it is possible that additional mechanisms of neovascularization also exist. One possibility is that *in vivo*, bone marrow–derived (BMD) progenitor cells are recruited to the tumor. Indeed, BMD endothelial progenitors can incorporate into the luminal walls of neovessels during breast cancer progression (30) and inhibition of BMD endothelial progenitor cell mobilization/function has been shown to decrease tumor vascularization (30, 31). Given the role of Nodal in the regulation of stem cell fate and morphogenesis, it is conceivable that it also regulates the recruitment of endothelial progenitors.

To recapitulate therapeutic intervention, we designed an assay wherein Nodal was inhibited after tumor initiation. We found that there was a decrease in vascularization when Nodal was inhibited in these tumors. In accordance with these observations, one study in melanoma showed a decrease in lung colonization following administration of a function-blocking antibody targeted to Nodal (32). Colonies that formed in mice treated with anti-Nodal antibody exhibited signs of apoptosis inclusive of cytoplasmic swelling and vacuole expansion; however, the antiangiogenic effects of Nodal inhibition was not directly explored. We suggest that Nodal inhibition reduced tumor growth, at least in part, by preventing angiogenesis.

It is not clear from our experiments whether vascular reduction via Nodal inhibition would yield a positive or negative response with respect to metastasis, particularly given our findings that Nodal knockdown results in tumor hypoxia. Tumor hypoxia is associated with cellular programs that yield enhanced metastasis. Moreover, hypoxia promotes tumor-initiating cell populations (33) and induces therapeutic resistance to chemotherapy and radiation (34, 35). Furthermore, overexpression of hypoxia-inducible factor α (HIF-1α) promotes metastatic phenotypes and is associated with increased breast cancer relapse and decreased patient survival (36–38). HIF proteins also upregulate of a number of stem cell–associated transcription factors that induce tumor-promoting programs, including TWIST1 and ZEB1/2 (39–43). We show that Nodal inhibition causes decreased VEGF expression and increased tumor necrosis concomitant with tumor hypoxia; however, we have previously shown that hypoxia induces Nodal expression through HIF-1α (20), and VEGF is one of the best-characterized targets of HIF proteins (44). Hence, studies that measure metastases following Nodal inhibition and that target Nodal and hypoxia in combination warrant investigation.

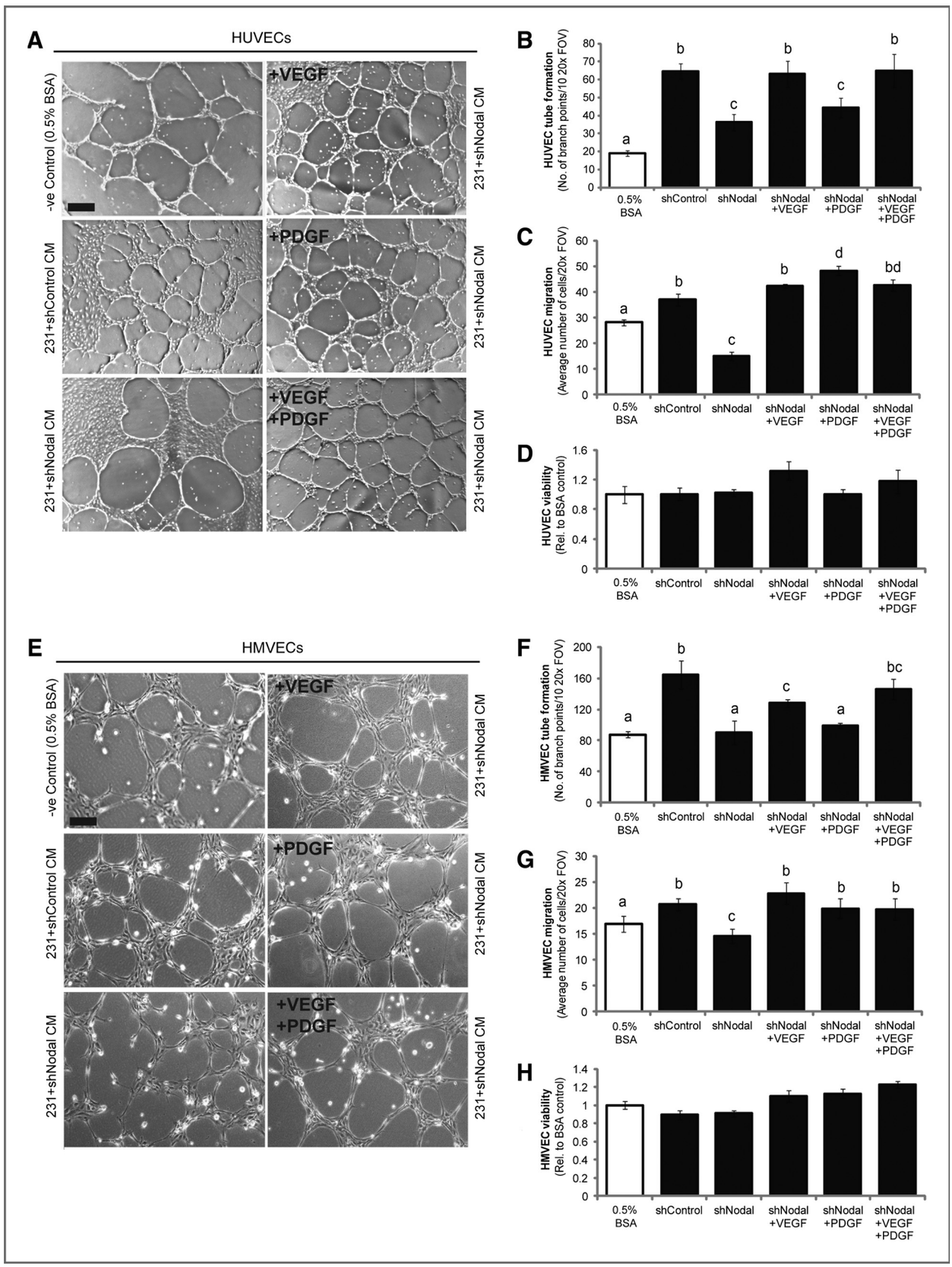
A
HUVECs
-ve Control (0.5% BSA)
231+shControl CM
231+shNodal CM
+VEGF
+PDGF
+VEGF
+PDGF
231+shNodal CM
B
HUVEC tube formation
(No. of branch points/10 20x FOV)
C
HUVEC migration
(Average number of cells/20x FOV)
D
HUVEC viability
(Rel. to BSA control)
0.5% BSA
shControl
shNodal
shNodal +VEGF
shNodal +PDGF
shNodal +VEGF +PDGF
E
HMVECs
F
HMVEC tube formation
(No. of branch points/10 20x FOV)
G
HMVEC migration
(Average number of cells/20x FOV)
H
HMVEC viability
(Rel. to BSA control)

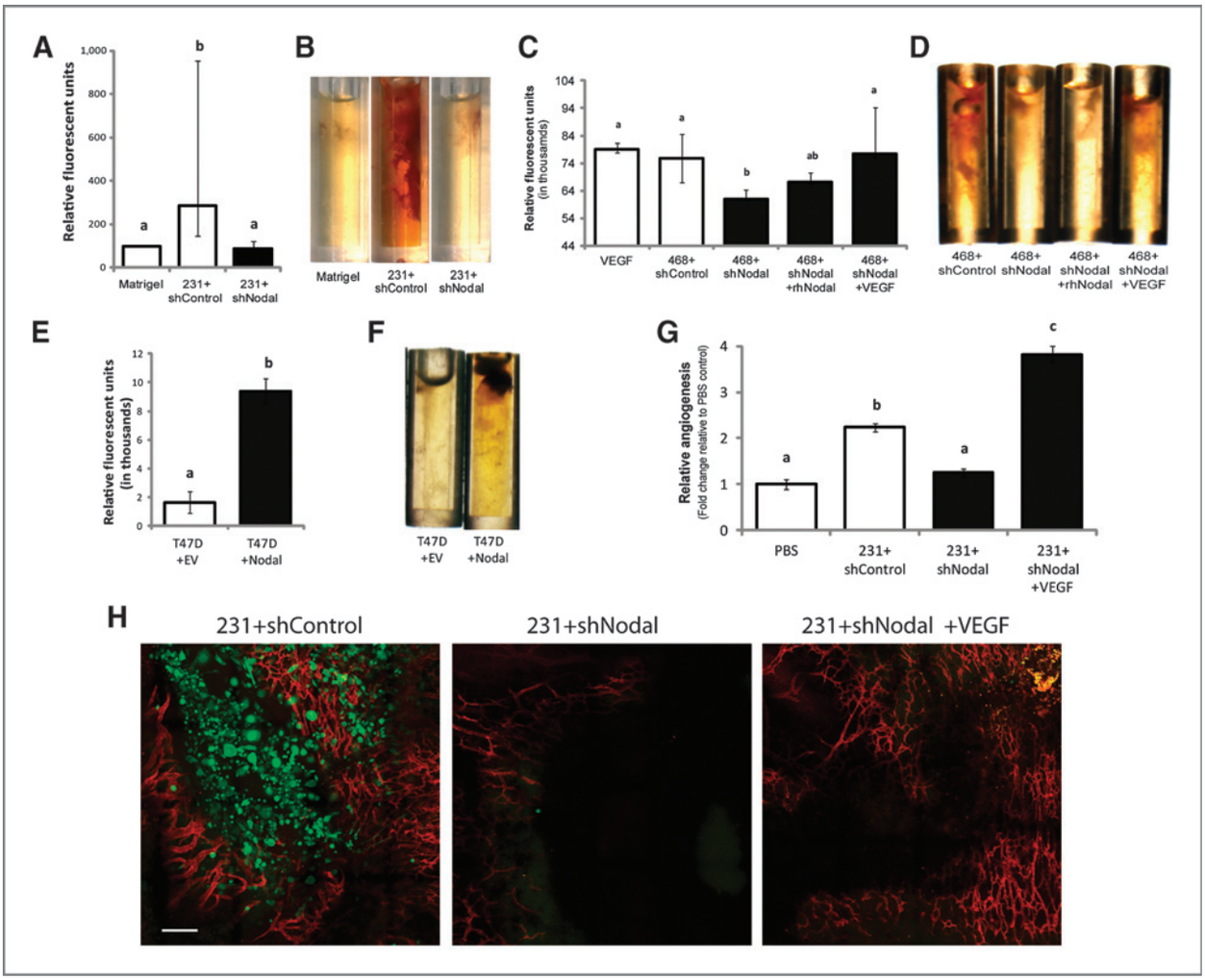

Figure 5. Nodal promotes vascular recruitment *in vivo*. A, DIVAAs were conducted with 231+shNodal or 231+shControl cells. Nodal knockdown caused a significant reduction in vascular recruitment compared with 231+shControl. Data are nonparametric and are presented as median ± interquartile range ($n = 10$, $P = 0.003$). B, images of representative angioreactors corresponding to A. C, DIVAAs were conducted with 468+shNodal cells or 468+shControl cells. 468+shNodal cells had significantly reduced vascular recruitment compared with 468+shControl cells. This effect was partially rescued by the addition of rhNodal to angioreactors containing 468+shNodal cells and was rescued by the addition of VEGF. Recombinant VEGF in Matrigel (no cells) was included as a control. Data are presented as mean relative fluorescent units ± SEM ($n = 7$, $P < 0.007$). D, images of representative angioreactors corresponding to C. E, DIVAAs were conducted with T47D+Nodal or T47D+EV–transfected cells. Bars represent mean relative fluorescent units ± SEM ($n = 10$, $P < 0.001$). F, images of representative angioreactors corresponding to E. G, 231+shControl cells, 231+shNodal cells, or 231+shNodal cells +VEGF were inoculated onto chick CAMs with a collagen mesh grid. After 3 days, 231+shControl cells induced significantly more angiogenesis compared with 231+shNodal cells. This effect was rescued by the addition of VEGF to 231+shNodal cells. Bars represent mean angiogenesis relative to a PBS control ± SEM ($n \geq 37$, $P < 0.001$). H, confocal images of a 5-day tumor assay carried out on chick CAMs. 231+shControl cells formed large tumors compared with 231+shNodal cells. Inclusion of recombinant VEGF to 231+shNodal tumors did not rescue tumor formation. Vessels are shown in red, and cells are GFP labeled (green). Bar, 50 μm. For all graphs, superscripted letters have a statistical difference.

Collectively, we have shown that Nodal supports a pro-angiogenic niche. This discovery provides mechanistic insight into recent studies showing that cancer cells expressing stem cell–associated genes are better able to recruit vasculature than more differentiated cancer cells (13). Importantly, we have shown that Nodal is correlated with high MVD in human breast cancers, and that blocking Nodal expression in established tumors results in a marked

Figure 4. VEGF and PDGF rescue the effects of Nodal knockdown on angiogenic phenotypes. A, representative images of HUVEC tube formation in cells treated with 5% BSA, 231+shControl-conditioned media, 231+shNodal-conditioned media, or 231+shNodal-conditioned media + VEGF and/or PDGF. Bar, 100 μm. B, quantified HUVEC tube formation corresponding to A. Bars represent mean number of branch points ± SEM ($n = 3$, $P < 0.001$). C, HUVEC cellular migration in response to treatments from A and B. Bars represent mean number of migrated cells per FOV ± SEM ($n = 4$, $P < 0.001$). D, viability of HUVECs in response to treatments from A–C. Bars represent fold change in fluorescence ± SEM relative to 5% BSA control ($n \geq 4$, $P = 0.2$). E, representative images of HMVEC tube formation in cells treated with 5% BSA, 231+shControl-conditioned media, 231+shNodal-conditioned media, or 231+shNodal-conditioned media + VEGF and/or PDGF. Bar, 50 μm. F, quantified HMVEC tube formation corresponding to E. Bars represent mean number of branch points ± SEM ($n = 3$, $P < 0.001$). G, HMVEC cellular migration in response to treatments from E and F. Bars represent mean number of migrated cells per FOV ± SEM ($n = 4$, $P < 0.001$). H, viability of HMVECs in response to treatment conditions from E–G. Bars represent fold change in fluorescence ± SEM relative to 5% BSA control ($n = 6$, $P > 0.05$). For all graphs, superscripted letters indicate a statistical difference as specified. BSA, bovine serum albumin; CM, conditioned media; FOV, field of view.

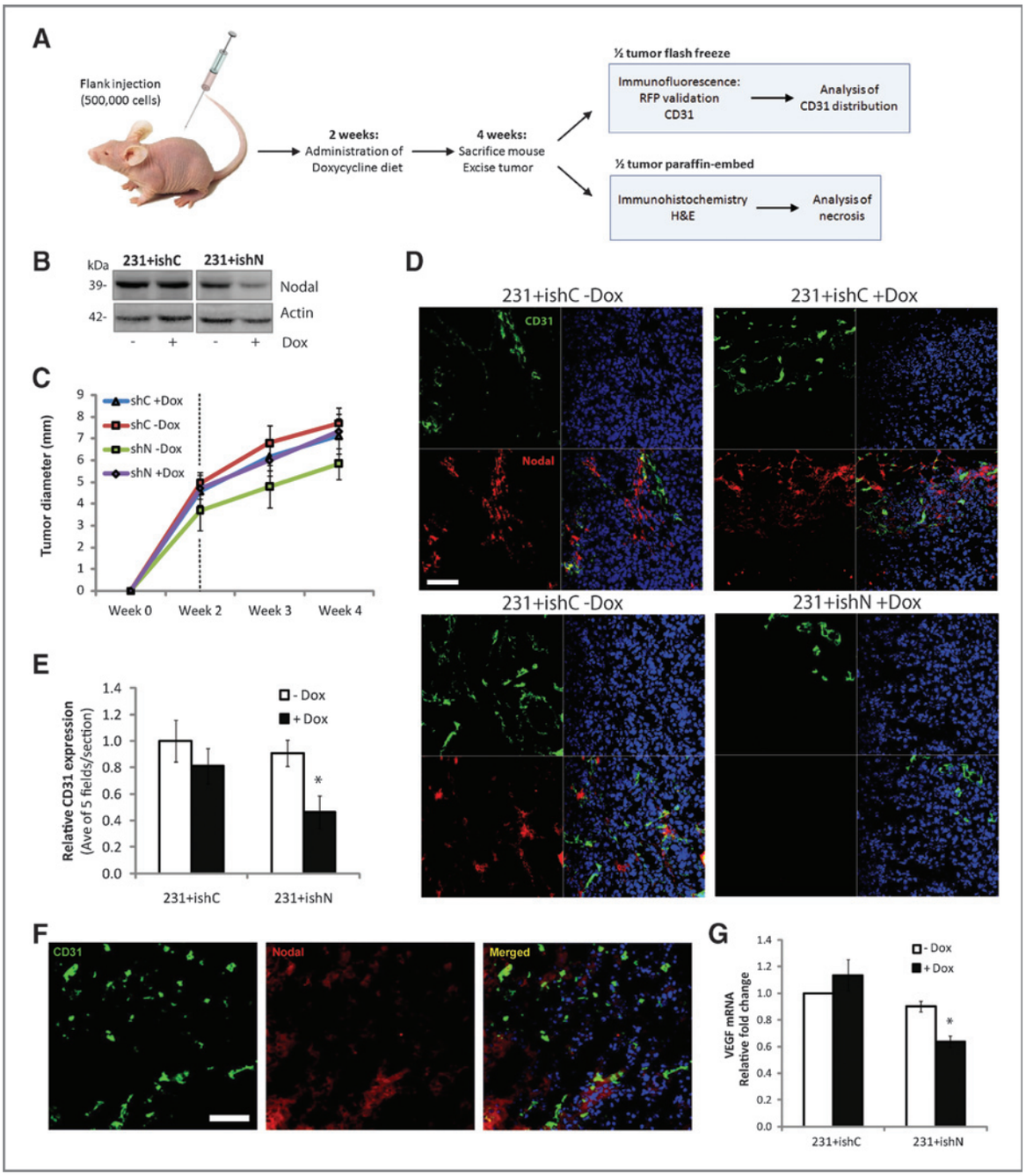

Figure 6. Nodal inhibition following tumor formation causes a reduction of tumor vascularization. A, schematic representation of inducible shRNA tumor model. A total of 500,000 doxycycline-inducible 231+ishC or 213+ishN stably transfected cells were injected into nude mice. Mice were given normal chow (–Dox) or normal chow for 2 weeks followed by doxycyclin-chow for 2 weeks (+Dox). After 4 weeks, tumors were excised and cryosectioned for immunofluorescence or paraffin-embedded for H&E. B, Western blot analysis confirmed that the shRNA constructs were efficiently transfected and operated as expected in response to doxycyclin *in vitro*. Pro-Nodal (~39 kDa) is depicted and actin is used as a loading control. C, tumor diameter over the course of 4 weeks, following flank injection with 231+ishC or 231+ishN cells. Values represent mean tumor diameter (mm) at each time point ± SEM ($n \geq 4$, $P = 0.4$). The time at which doxycycline was administered is indicated by the dotted line. D, representative images used to assess CD31 (green) and Nodal (red) localization. 4′, 6-Diamidino-2-phenylindole (DAPI; blue) was used to stain the nuclei. Merged images are shown for each treatment. Bar, 50 μm. E, relative quantification of CD31 expression in excised 231+ishC- and 231+ishN–derived tumors. Values represent mean CD31 expression relative to 231+ishC –Dox tumors ± SEM, and the asterisk (*) indicates a significant difference compared with 231+ishC –Dox control ($n \geq 4$, $P = 0.04$). F, representative images of CD31 (green) and Nodal (red) in a 231+shN +Dox tumor in which Nodal was reexpressed. DAPI (blue) was used to stain the nuclei. Bar, 50 μm. G, real-time RT-PCR analysis of *VEGF* expression in 231+ishC- and 231+ishN–derived tumors. Expression levels are normalized to HPRT1. Bars represent mean gene expression ± SEM relative to 231+shC –Dox, and * indicates a significant difference compared with 231+ishC –Dox ($n \geq 3$, $P = 0.003$).

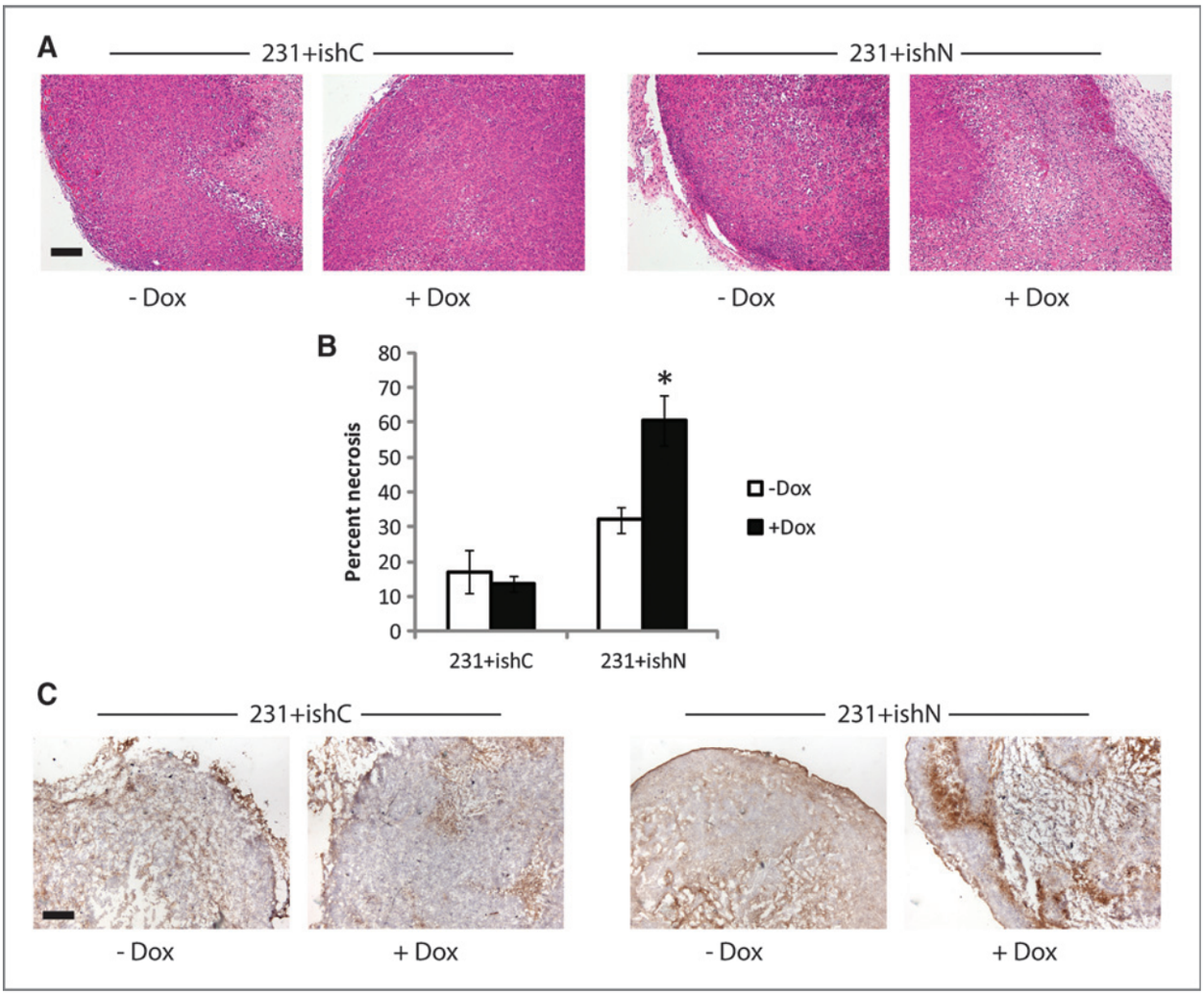

Figure 7. Nodal inhibition following tumor formation induces tumor necrosis and hypoxia. A, representative H&E images of tumors from 231+ishC and 231+ishN cells, with or without doxycycline chow, showing areas of tumor necrosis. Bar, 100 μm. B, quantification of necrosis corresponding to A. Bars represent mean percent necrosis of total tumor area ± SEM and the asterisk (*) indicates a significant difference compared with 231+ishC –Dox control ($n \geq 4$, $P < 0.001$). C, representative images of tumor hypoxia (brown) across treatment groups. Bar equals 50 μm. Dox, doxycycline.

reduction in vascularization concomitant with tumor necrosis. Our discovery suggests a novel role for Nodal as a target for the treatment of breast cancer.

Disclosure of Potential Conflicts of Interest

No potential conflicts of interest were disclosed.

Authors' Contributions

Conception and design: D.F. Quail, G. Zhang, D.A. Hess, L.-M. Postovit
Development of methodology: D.F. Quail, L.A. Walsh, G. Zhang, D.A. Hess, L.-M. Postovit
Acquisition of data (provided animals, acquired and managed patients, provided facilities, etc.): D.F. Quail, L.A. Walsh, G. Zhang, S.D. Findlay, J. Moreno, L. Fung, D.A. Hess
Analysis and interpretation of data (e.g., statistical analysis, biostatistics, computational analysis): D.F. Quail, L.A. Walsh, G. Zhang, J. Moreno, L. Fung, A. Ablack, J. Lewis, S.J. Done, D.A. Hess, L.-M. Postovit
Writing, review, and/or revision of the manuscript: D.F. Quail, L.A. Walsh, G. Zhang, A. Ablack, J. Lewis, S.J. Done, D.A. Hess, L.-M. Postovit
Administrative, technical, or material support (i.e., reporting or organizing data, constructing databases): D.F. Quail, D.A. Hess
Study supervision: L.-M. Postovit

Grant Support

This work was supported by the Canadian Institutes for Health Research (MOP 89714, MOP 119589, and PLS 95381) and the Cancer Research Society to L.-M. Postovit. D.F. Quail is supported by fellowships from the Canadian Breast Cancer Foundation and a CIHR training grant. L.A. Walsh is a recipient of a Natural Sciences and Engineering Research Council Alexander Graham Bell Canada Graduate Scholarship. J. Moreno is supported by the Terry Fox Foundation Strategic Health Research Training Program in Cancer Research at CIHR (TGT-53912). L.-M. Postovit is the recipient of the Premier New Investigator Award from the CIHR. D.A. Hess is the recipient of a new investigator award and MacDonald Scholarship for the Canadian Heart and Stroke Foundation.

The costs of publication of this article were defrayed in part by the payment of page charges. This article must therefore be hereby marked *advertisement* in accordance with 18 U.S.C. Section 1734 solely to indicate this fact.

Received December 3, 2011; revised April 26, 2012; accepted May 16, 2012; published August 1, 2012.

References

1. Hendrix MJ, Seftor EA, Seftor RE, Kasemeier-Kulesa J, Kulesa PM, Postovit LM. Reprogramming metastatic tumour cells with embryonic microenvironments. Nat Rev Cancer 2007;7:246–55.
2. Reya T, Morrison SJ, Clarke MF, Weissman IL. Stem cells, cancer, and cancer stem cells. Nature 2001;414:105–11.
3. Ben-Porath I, Thomson MW, Carey VJ, Ge R, Bell GW, Regev A, et al. An embryonic stem cell-like gene expression signature in poorly differentiated aggressive human tumors. Nat Genet 2008;40: 499–507.
4. Hendrix MJ, Seftor EA, Hess AR, Seftor RE. Vasculogenic mimicry and tumour-cell plasticity: lessons from melanoma. Nat Rev Cancer 2003; 3:411–21.
5. Topczewska JM, Postovit LM, Margaryan NV, Sam A, Hess AR, Wheaton WW, et al. Embryonic and tumorigenic pathways converge via Nodal signaling: role in melanoma aggressiveness. Nat Med 2006;12:925–32.
6. Postovit LM, Margaryan NV, Seftor EA, Kirschmann DA, Lipavsky A, Wheaton WW, et al. Human embryonic stem cell microenvironment suppresses the tumorigenic phenotype of aggressive cancer cells. Proc Natl Acad Sci U S A 2008;105:4329–34.
7. Lee CC, Jan HJ, Lai JH, Ma HI, Hueng DY, Gladys Lee YC, et al. Nodal promotes growth and invasion in human gliomas. Oncogene 2010; 29:3110–23.
8. Schier AF. Nodal signaling in vertebrate development. Annu Rev Cell Dev Biol 2003;19:589–621.
9. Lonardo E, Hermann PC, Mueller MT, Huber S, Balic A, Miranda-Lorenzo I, et al. Nodal/Activin signaling drives self-renewal and tumorigenicity of pancreatic cancer stem cells and provides a target for combined drug therapy. Cell Stem Cell 2011;9:433–46.
10. Lawrence MG, Margaryan NV, Loessner D, Collins A, Kerr KM, Turner M, et al. Reactivation of embryonic nodal signaling is associated with tumor progression and promotes the growth of prostate cancer cells. Prostate 2011;71:1198–209.
11. Grange C, Tapparo M, Collino F, Vitillo L, Damasco C, Deregibus MC, et al. Microvesicles released from human renal cancer stem cells stimulate angiogenesis and formation of lung premetastatic niche. Cancer Res 2011;71:5346–56.
12. Phillips HS, Kharbanda S, Chen R, Forrest WF, Soriano RH, Wu TD, et al. Molecular subclasses of high-grade glioma predict prognosis, delineate a pattern of disease progression, and resemble stages in neurogenesis. Cancer Cell 2006;9:157–73.
13. Folkins C, Shaked Y, Man S, Tang T, Lee CR, Zhu Z, et al. Glioma tumor stem-like cells promote tumor angiogenesis and vasculogenesis via vascular endothelial growth factor and stromal-derived factor 1. Cancer Res 2009;69:7243–51.
14. Hueng DY, Lin GJ, Huang SH, Liu LW, Ju DT, Chen YW, et al. Inhibition of Nodal suppresses angiogenesis and growth of human gliomas. J Neurooncol 2011;104:21–31.
15. Hooijkaas AI, Gadiot J, van BH, Blank C. Expression of the embryological morphogen Nodal in stage III/IV melanoma. Melanoma Res 2011;21:491–501.
16. Papageorgiou I, Nicholls PK, Wang F, Lackmann M, Makanji Y, Salamonsen LA, et al. Expression of nodal signalling components in cycling human endometrium and in endometrial cancer. Reprod Biol Endocrinol 2009;7:122.
17. Allred DC, Harvey JM, Berardo M, Clark GM. Prognostic and predictive factors in breast cancer by immunohistochemical analysis. Mod Pathol 1998;11:155–68.
18. Vermeulen PB, Gasparini G, Fox SB, Toi M, Martin L, McCulloch P, et al. Quantification of angiogenesis in solid human tumours: an international consensus on the methodology and criteria of evaluation. Eur J Cancer 1996;32A:2474–84.
19. Le Good JA, Joubin K, Giraldez AJ, Ben-Haim N, Beck S, Chen Y, et al. Nodal stability determines signaling range. Curr Biol 2005;15:31–6.
20. Quail DF, Taylor MJ, Walsh LA, Dieters-Castator D, Das P, Jewer M, et al. Low oxygen levels induce the expression of the embryonic morphogen nodal. Mol Biol Cell 2011;22:4809–21.
21. Ling MT, Lau TC, Zhou C, Chua CW, Kwok WK, Wang Q, et al. Overexpression of Id-1 in prostate cancer cells promotes angiogenesis through the activation of vascular endothelial growth factor (VEGF). Carcinogenesis 2005;26:1668–76.
22. Reinmuth N, Rensinghoff S, Raedel M, Fehrmann N, Schwoppe C, Kessler T, et al. Paracrine interactions of vascular endothelial growth factor and platelet-derived growth factor in endothelial and lung cancer cells. Int J Oncol 2007;31:621–6.
23. Leong HS, Steinmetz NF, Ablack A, Destito G, Zijlstra A, Stuhlmann H, et al. Intravital imaging of embryonic and tumor neovasculature using viral nanoparticles. Nat Protoc 2010;5:1406–17.
24. Naumov GN, Akslen LA, Folkman J. Role of angiogenesis in human tumor dormancy: animal models of the angiogenic switch. Cell Cycle 2006;5:1779–87.
25. Sauer G, Deissler H. Angiogenesis: prognostic and therapeutic implications in gynecologic and breast malignancies. Curr Opin Obstet Gynecol 2003;15:45–9.
26. Guedez L, Rivera AM, Salloum R, Miller ML, Diegmueller JJ, Bungay PM, et al. Quantitative assessment of angiogenic responses by the directed *in vivo* angiogenesis assay. Am J Pathol 2003;162:1431–9.
27. Constam DB. Riding shotgun: a dual role for the epidermal growth factor-Cripto/FRL-1/Cryptic protein Cripto in Nodal trafficking. Traffic 2009;10:783–91.
28. Adkins HB, Bianco C, Schiffer SG, Rayhorn P, Zafari M, Cheung AE, et al. Antibody blockade of the Cripto CFC domain suppresses tumor cell growth *in vivo*. J Clin Invest 2003;112:575–87.
29. Bianco C, Strizzi L, Ebert A, Chang C, Rehman A, Normanno N, et al. Role of human cripto-1 in tumor angiogenesis. J Natl Cancer Inst 2005;97:132–41.
30. Nolan DJ, Ciarrocchi A, Mellick AS, Jaggi JS, Bambino K, Gupta S, et al. Bone marrow-derived endothelial progenitor cells are a major determinant of nascent tumor neovascularization. Genes Dev 2007; 21:1546–58.
31. Gao D, Nolan DJ, Mellick AS, Bambino K, McDonnell K, Mittal V. Endothelial progenitor cells control the angiogenic switch in mouse lung metastasis. Science 2008;319:195–8.
32. Strizzi L, Postovit LM, Margaryan NV, Lipavsky A, Gadiot J, Blank C, et al. Nodal as a biomarker for melanoma progression and a new therapeutic target for clinical intervention. Expert Rev Dermatol 2009; 4:67–78.
33. Schwab LP, Peacock DL, Majumdar D, Ingels JF, Jensen LC, Smith KD, et al. Hypoxia inducible factor-1alpha promotes primary tumor growth and tumor-initiating cell activity in breast cancer. Breast Cancer Res 2012;14:R6.
34. Cosse JP, Michiels C. Tumour hypoxia affects the responsiveness of cancer cells to chemotherapy and promotes cancer progression. Anticancer Agents Med Chem 2008;8:790–7.
35. Rockwell S, Dobrucki IT, Kim EY, Marrison ST, Vu VT. Hypoxia and radiation therapy: past history, ongoing research, and future promise. Curr Mol Med 2009;9:442–58.
36. Gort EH, Groot AJ, van der WE, van Diest PJ, Vooijs MA. Hypoxic regulation of metastasis via hypoxia-inducible factors. Curr Mol Med 2008;8:60–7.
37. Chi JT, Wang Z, Nuyten DS, Rodriguez EH, Schaner ME, Salim A, et al. Gene expression programs in response to hypoxia: cell type specificity and prognostic significance in human cancers. PLoS Med 2006;3:e47.
38. Dales JP, Garcia S, Meunier-Carpentier S, Andrac-Meyer L, Haddad O, Lavaut MN, et al. Overexpression of hypoxia-inducible factor HIF-1alpha predicts early relapse in breast cancer: retrospective study in a series of 745 patients. Int J Cancer 2005;116:734–9.
39. Yang MH, Wu KJ. TWIST activation by hypoxia inducible factor-1 (HIF-1): implications in metastasis and development. Cell Cycle 2008;7:2090–6.
40. Yang MH, Wu MZ, Chiou SH, Chen PM, Chang SY, Liu CJ, et al. Direct regulation of TWIST by HIF-1alpha promotes metastasis. Nat Cell Biol 2008;10:295–305.
41. Peinado H, Cano A. A hypoxic twist in metastasis. Nat Cell Biol 2008;10:253–4.
42. Katoh M, Katoh M. Integrative genomic analyses of ZEB2: Transcriptional regulation of ZEB2 based on SMADs, ETS1,

HIF1alpha, POU/OCT, and NF-kappaB. Int J Oncol 2009;34: 1737–42.

43. Krishnamachary B, Zagzag D, Nagasawa H, Rainey K, Okuyama H, Baek JH, et al. Hypoxia-inducible factor-1-dependent repression of E-cadherin in von Hippel-Lindau tumor suppressor-null renal cell carcinoma mediated by TCF3, ZFHX1A, and ZFHX1B. Cancer Res 2006;66:2725–31.
44. Shweiki D, Itin A, Soffer D, Keshet E. Vascular endothelial growth factor induced by hypoxia may mediate hypoxia-initiated angiogenesis. Nature 1992;359:843–5.